Lethal arrhythmias in *Tbx3*-deficient mice reveal extreme dosage sensitivity of cardiac conduction system function and homeostasis

Deborah U. Frank[a], Kandis L. Carter[a], Kirk R. Thomas[b], R. Michael Burr[a], Martijn L. Bakker[c], William A. Coetzee[d], Martin Tristani-Firouzi[a], Michael J. Bamshad[e], Vincent M. Christoffels[c], and Anne M. Moon[a,b,1]

[a]Department of Pediatrics and [b]Molecular Medicine Program, University of Utah, Salt Lake City, UT 84158; [c]Department of Anatomy, Embryology and Physiology, Academic Medical Center, University of Amsterdam, 1012 WX Amsterdam, The Netherlands; [d]Department of Pediatrics, New York University, New York, NY 10016; and [e]Department of Pediatrics, University of Washington, Seattle, WA 98195

TBX3 is critical for human development: mutations in TBX3 cause congenital anomalies in patients with ulnar-mammary syndrome. Data from mice and humans suggest multiple roles for Tbx3 in development and function of the cardiac conduction system. The mechanisms underlying the functional development, maturation, and maintenance of the conduction system are not well understood. We tested the requirements for Tbx3 in these processes. We generated a unique series of *Tbx3* hypomorphic and conditional mouse mutants with varying levels and locations of Tbx3 activity within the heart, and developed techniques for evaluating in vivo embryonic conduction system function. Disruption of *Tbx3* function in different regions of the developing heart causes discrete phenotypes and lethal arrhythmias: sinus pauses and bradycardia indicate sinoatrial node dysfunction, whereas preexcitation and atrioventricular block reveal abnormalities in the atrioventricular junction. Surviving *Tbx3* mutants are at increased risk for sudden death. Arrhythmias induced by knockdown of *Tbx3* in adults reveal its requirement for conduction system homeostasis. Arrhythmias in *Tbx3*-deficient embryos are accompanied by disrupted expression of multiple ion channels despite preserved expression of previously described conduction system markers. These findings indicate that Tbx3 is required for the conduction system to establish and maintain its correct molecular identity and functional properties. In conclusion, Tbx3 is required for the functional development, maturation, and homeostasis of the conduction system in a highly dosage-sensitive manner. *TBX3* and its regulatory targets merit investigation as candidates for human arrhythmias.

heart rhythm | heart development | embryonic electrocardiogram | tissue regeneration

The cardiac conduction system (CCS) comprises the sinoatrial node (SAN), atrioventricular node (AVN), atrioventricular (AV) bundle (AVB), bundle branches, and Purkinje fibers. These tissues initiate and propagate electrical depolarization to generate synchronized chamber contraction. The molecular and electrophysiological properties of CCS tissues are distinct from working myocardium, and individual components of the CCS have unique features that reflect their specialized functions (1–4).

Arrhythmias are primary indicators of CCS dysfunction, which manifests as disrupted SAN pacing, blocked AVN conduction, or slow ventricular activation. Preexcitation or reentrant arrhythmias indicate ectopic pathways or abnormal insulation of the AV components (5). Arrhythmias can be congenital or acquired, and mutations in genes encoding molecules required for CCS development or directly involved in conduction (ion channel subunits or gap junction proteins) have been identified (6).

Multiple *Tbx* genes are expressed in the developing CCS in mice and mutations in *TBX3* and *TBX5* have been associated with human CCS dysfunction (1, 6, 7). Mutations in *TBX3* cause human ulnar-mammary syndrome (UMS), characterized by limb malformations, apocrine and mammary gland hypoplasia, and dental and genital abnormalities (8). Cardiac structural defects

have been reported in two patients with UMS, one with the Wolff–Parkinson–White syndrome conduction abnormality (7, 9). *TBX3* expression was decreased in the hearts of patients with right ventricular outflow tract tachycardia, and variability in the *TBX5–TBX3* region correlates with PR interval duration (10, 11). In the myocardium, *Tbx3* is predominantly expressed in the developing and mature pacemakers [SAN and AV canal (AVC) and node] and the AVB and branches (12). Tbx3 is sufficient to induce the formation of ectopic pacemakers in the atrial myocardium during development (13). These data suggest a role for *Tbx3* in mammalian cardiac development and CCS function.

Embryonic lethality of previously reported *Tbx3* mutants precluded testing whether, or in what tissues, Tbx3 is required for CCS development or maintenance. To overcome this, we generated a unique *Tbx3* allelic series and performed temporospatially regulated conditional *Tbx3* ablations. Because methods to assay electrophysiologic function of embryos in vivo were lacking, we developed techniques to evaluate prenatal cardiac conduction including noninvasive echocardiograms and direct ECG recordings. We found that development of the structural and functional characteristics of the CCS is extremely sensitive to Tbx3 such that decreasing the amount of Tbx3 below a critical level causes lethal embryonic arrhythmias. Furthermore, we discovered that Tbx3 is also required for the homeostasis of the adult CCS.

Results

Prenatal Survival Is Sensitive to *Tbx3* mRNA Dosage. We created graded increments in *Tbx3* mRNA production by combining different gene-targeted *Tbx3* alleles: $Tbx3^{GH}$, $Tbx3^{G}$, $Tbx3^{flox}$, $Tbx3^{\Delta flox}$, and $Tbx3^{N}$ (Fig. 1 *A* and *B*). These incremental changes in *Tbx3* mRNA revealed that prenatal survival is markedly sensitive to *Tbx3* dosage.

The $Tbx3^{GH}$ allele was hypomorphic relative to the WT allele in terms of mRNA production (Fig. 1*B*), and there was markedly decreased *Tbx3* mRNA and protein in $Tbx3^{GH/N}$ compound heterozygotes (Figs. 1*B* and 2 *E–H*). This is caused, at least in part, by aberrant splicing into GFP, which we could detect immunohistochemically and by RT-PCR. Although the location of Tbx3 expression was the same in hypomorphs and controls, the Tbx3^{+}

A Tbx3 allelic series

B Tbx3 mRNA

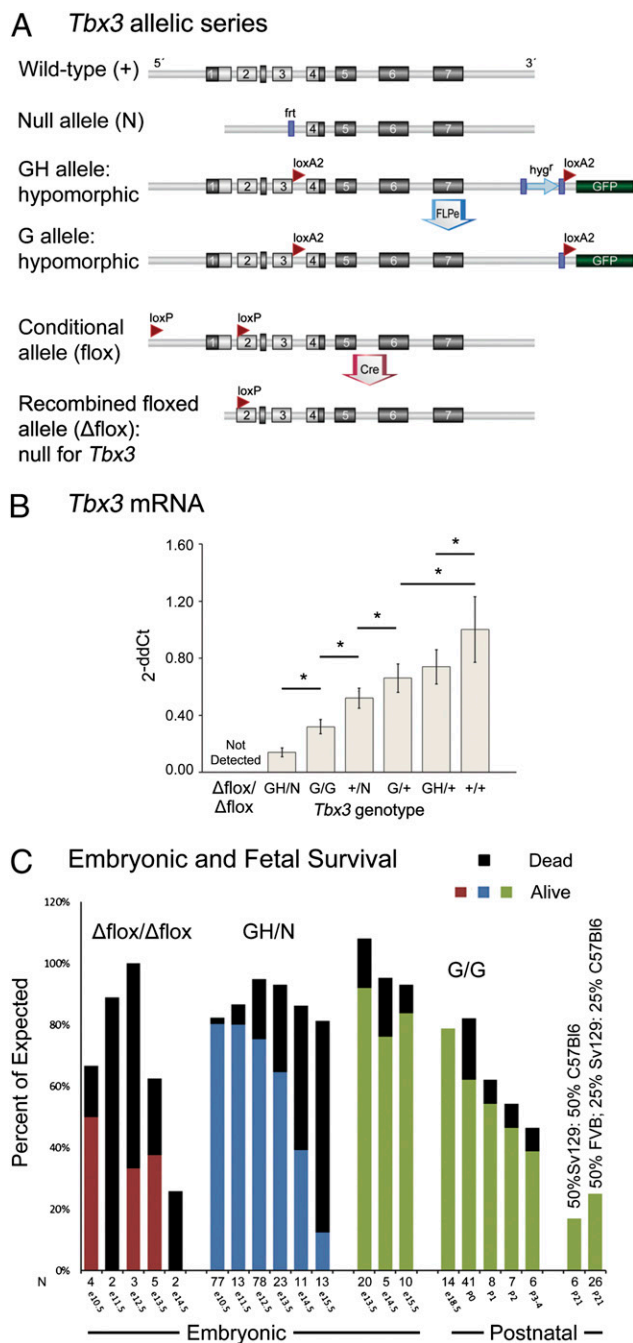## C Embryonic and Fetal Survival

Fig. 1. An allelic series allows for incremental changes in Tbx3 expression. (*A*) *Tbx3*-targeted alleles described in this study. Light gray denotes DNA binding domain exons, and other exons are dark gray. (*B*) qRT-PCR of *Tbx3* mRNA levels. Statistical analysis was by ANOVA with $P < 0.001$ for differences between genotypes. Asterisk indicates difference between pairs of genotypes by Student–Newman–Keuls test ($P < 0.05$). (*C*) Survival curves show *Tbx3* dose dependence. Percentages reflect expected number of mutants from mating heterozygous mice or for $Tbx3^{GH/N}$ from mating a $Tbx3^{GH/+}$ female with a $Tbx3^{+/N}$ male.

domains were smaller in the mutants and staining intensity per cell was decreased (Fig. S1). Most $Tbx3^{GH/N}$ hypomorphs (background 50% Sv129; 50% C57Bl6) died between embryonic day (E) 13.5 and E15.5; none survived to birth (Fig. 1*C*). $Tbx3^{GH/N}$ mutants had limb abnormalities similar to $Tbx3^{tm1Pa/tm1Pa}$ mutants (14) (Fig. S2). Removal of the hygromycin resistance gene from $Tbx3^{GH}$ generated the $Tbx3^{G}$ allele (Fig. 1*A*). $Tbx3^{G}$ was also hypomorphic and

the level of *Tbx3* mRNA in $Tbx3^{G/G}$ homozygotes was intermediate to that in $Tbx3^{+/N}$ heterozygotes and $Tbx3^{GH/N}$ compound heterozygotes (Fig. 1*B*). Notably, this increase in *Tbx3* function permitted 80% of $Tbx3^{G/G}$ mice to survive to birth. Progressive postnatal loss resulted in an 11% survival rate to adulthood (Fig. 1*C*).

These findings in hypomorphs are distinct from the previously reported *Tbx3* loss-of-function (LOF) mouse mutants: $Tbx3^{tm1Pa/tm1Pa}$, $Tbx3^{Cre/Cre}$, and $Tbx3^{neo/neo}$ (13–15). There is significant phenotypic variability among the previously reported lines, the etiology of which is unknown. Our $Tbx3^{N}$ allele deletes the DNA binding domain similar to the allele reported by Davenport et al. (14), which die between E11 and E16, yet most of our $Tbx3^{N/N}$ mutants died before E10.5 (56% of expected mutants were present at E10.5, 25% of those recovered were dead; $n = 11$ litters). $Tbx3^{N/N}$ cardiac morphology was similar to that reported by Ribeiro et al. (15). Both sexes of our $Tbx3^{+/N}$ mice demonstrated reduced fertility, and mothers had poor nurturing, likely because of the requirements for Tbx3 in genital and mammary development (8, 14); thus, $Tbx3^{N/N}$ mutants were exceedingly difficult to generate and not further evaluated. We therefore converted a unique conditional allele ($Tbx3^{flox}$) into a null allele ($Tbx3^{\Delta flox}$) by using deleter-Cre mice (16). *Tbx3* transcript and protein were undetectable in $Tbx3^{\Delta flox/\Delta flox}$ hearts (Figs. 1*B* and 2 *A*–*D*), and survival of $Tbx3^{\Delta flox\Delta/flox}$ mice was similar to other *Tbx3* reported LOF mutants, with none surviving to birth (Fig. 1*C*).

$Tbx3^{tm1Pa/tm1Pa}$ mouse mutants reportedly die from yolk sac degeneration (14). However, we detected no morphologic defects in the yolk sacs of $Tbx3^{GH/N}$ or $Tbx3^{G/G}$ mutants (Fig. S2). Other potential causes of midgestational death include hematopoietic failure, placental insufficiency, and cardiac failure. There was no evidence of the anemia or liver hypoplasia (Fig. S2) reported in $Tbx3^{Cre/Cre}$ LOF mutants (17). No differences were detected in embryo and placenta weights, or placental histology (Fig. S2), between $Tbx3^{GH/N}$ and $Tbx3^{+/+}$ control littermates. Thus, we could not attribute the lethality of these mutants to yolk sac, hematopoietic, or placental defects. The timing of death and their edematous appearance (Fig. S2) suggested cardiovascular insufficiency as the likely pathogenic mechanism.

A total of 85% of $Tbx3^{GH/N}$ E13.5 to E14.5 hypomorphs had large interventricular foramina ($n = 7$) compared with the closed foramina in 85% of littermate controls ($n = 13$). Atrial–ventricular alignments were normal, and only rare cases of ventricular–arterial malalignment were present ($n = 2$). Both these defects are well tolerated prenatally in many different mouse models (18), thus eliminating cardiac structural abnormalities as the cause of universal $Tbx3^{GH/N}$ embryonic lethality.

In utero echocardiography was performed serially on *Tbx3* mutants of different genotypes ($Tbx3^{\Delta flox/\Delta flox}$, $Tbx3^{GH/N}$, and $Tbx3^{G/G}$) and their littermates from E10.5 to E15.5. No Doppler blood flow abnormalities in umbilical or yolk sac vessels or at the AV or outflow tract cushions were detected, nor were there overall differences in heart rate or cardiac contractile function at these stages (Table S1). However, we identified severe arrhythmias, as detailed below.

***Tbx3* Mutants Had Pre- and Postnatal Arrhythmias.** Asynchronous atrial and ventricular contraction (an arrhythmia phenotype called AV block) was reproducibly detected in 2D (Movie S1 and Movie S2) and on Doppler echocardiography (Fig. 3*A*) in $Tbx3^{GH/N}$ hypomorphic embryos. This arrhythmia was not observed in littermates or in litters of WT embryos, indicating that it is attributable to decreased Tbx3 (Fig. S3). Echocardiographic detection of embryonic AV block has not previously been reported in mice to our knowledge, so we confirmed the electrophysiologic basis for asynchronous contractions by developing a method to directly record embryonic ECGs (Fig. 3*B*).

AV block occurred intermittently; embryos were found to have AV synchrony alternating with AV block of variable conduction
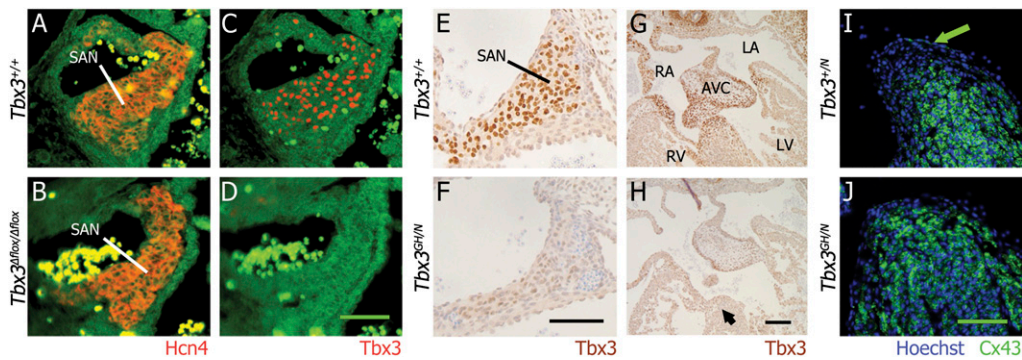
Frank et al.

www.manaraa.com

Fig. 2. Diminished Tbx3 and disrupted Cx43 protein in $Tbx3^{GH/N}$ hypomorphs. (*A–D*) E13.5 $Tbx3^{\Delta flox/\Delta flox}$ mutants do not express Tbx3 (*D*, absent red) in the Hcn4$^+$ (red) SAN region (*B*). (*E–H*) E12.5 $Tbx3^{GH/N}$ hypomorphs have decreased Tbx3 protein (brown) in the SAN (*F*) and AVC (*H*) regions compared with a WT littermate (*E* and *G*). Note severely decreased Tbx3 at the crest of the ventricular septum in the hypomorph (*H*, black arrow). (*I*) Cx43 (green) is normally excluded from the crest of the ventricular septum (green arrow). (*J*) Abnormal Cx43 expressed at ventricular septal crest in $Tbx3^{GH/N}$ hypomorph. LA, left atrium; LV, left ventricle; RA, right atrium; RV, right ventricle. (Scale bars: 50 μm.)

efficiency (2:1–5:1 block) during approximately 5 min of interrogation (Fig. S3). AV block was detected exclusively in mice with the lowest *Tbx3* expression levels ($Tbx3^{\Delta flox/flox}$, $Tbx3^{GH/N}$, and $Tbx3^{G/G}$) and is most closely associated with fetal demise. In serial studies, AV block and other arrhythmias were identified at E11.5 to E13.5 in mutants with embryonic demise occurring before the next daily study ($n = 5$) or by the time of euthanasia ($n = 2$; E15.5). In another cohort of embryos, AV block was detected on 2 to 3 consecutive days between E11.5 and E14.5 ($n = 7$ mutants), indicating that AV block was not merely a reflection of imminent death. We conclude that inadequate cardiac output due to AV block and ventricular bradycardia causes embryonic death of *Tbx3*-deficient mutants. AV block was first detectable at E11.5 in $Tbx3^{GH/N}$ hypomorphs, and occurred in 50% of these embryos at E12.5. With the incrementally higher *Tbx3* expression in $Tbx3^{G/G}$ mutants, AV block was not detected until E13.5 or later. $Tbx3^{\Delta flox/flox}$ null mutants also had AV block. They suffered from earlier demise, and thus few litters were serially studied.

Atrial arrhythmias were seen in all three classes of *Tbx3* mutants, and in their littermates (Fig. 3*C* and Fig. S3). As analysis of four litters of WT embryos between E10.5 and E13.5 revealed rare bradycardia, but never atrial arrhythmias or AV block, the atrial arrhythmias in mice heterozygous for *Tbx3* mutations are further evidence of the profound dosage sensitivity of the developing conduction system to *Tbx3*.

Direct ECG recordings of $Tbx3^{G/G}$ newborns revealed a prolonged QRS duration and multiple arrhythmias including atrial bradycardia, atrial arrhythmias, and second-degree AV block (Table 1 and Fig. 3*D*) in the absence of contractile dysfunction. No differences were detected in short-axis dimensions of left ventricular chamber or wall thickness between WT ($n = 19$) and $Tbx3^{G/G}$ ($n = 12$) littermates. In contrast to our observations at embryonic and early fetal stages, heart rates were significantly slower in $Tbx3^{G/G}$ newborns compared with WT littermates, and fractional shortening was increased, possibly in compensation for their relative bradycardia (Table 1). We evaluated $Tbx3^{G/G}$ mutants recovered at birth for anatomical malformations. One fourth of the mutants evaluated by serial sections had structural malformations ($n = 3$ in 13), including tetralogy of Fallot, ventricular septal defect, and interrupted inferior vena cava with azygous continuation. Structural defects are less severe and frequent than those reported in Tbx3$^{-/-}$ and $Tbx3^{Cre/Cre}$ embryos (19, 20).

We also recorded ECGs on the rare surviving adult $Tbx3^{G/G}$ mutants (50% FVB, 25% Sv129, 25% C57Bl6) and found a shortened PR interval and marked heart rate variability compared with WT and $Tbx3^{G/+}$ mice (Table 2). Nine percent of adult $Tbx3^{G/G}$ mutants ($n = 2$ of 22) had sudden death. Telemetric 24-h ECG

recordings revealed a variety of arrhythmias including sinus bradycardia, sinus pauses, premature atrial contractions, junctional rhythm, AV block, likely ventricular preexcitation, premature ventricular contractions, and ventricular couplets consistent with global CCS dysfunction (Table 2, Fig. 3, and Fig. S4). Our interpretation of the rhythm shown in Fig. 3*I* is that there is electrical preexcitation of the ventricle; an alternative interpretation we cannot exclude with the available data are AV dissociation. The median QRS duration was significantly longer in $Tbx3^{G/G}$ mice compared with $Tbx3^{+/+}$ mice, reflecting the widened QRS observed in the 50% of mutants with likely ventricular preexcitation. The trend toward a shorter median PR interval may also result from preexcitation in mutants. One third of these animals had bradycardia, resulting in a median HR of 608 beats/min in $Tbx3^{G/G}$ mutants compared with 691 beats/min in $Tbx3^{+/+}$ ($P = 0.06$).

CCS Hypoplasia and Aberrant Gene Expression in *Tbx3* Hypomorphs.
$Tbx3^{Cre/Cre}$ knock-in mutants were reported to have abnormally small SA nodes (13). We quantified the developing SAN in $Tbx3^{GH/N}$ and $Tbx3^{G/G}$ mutants by using Hcn4 IHC in E12.5 embryos and newborns, respectively. SAN volume in $Tbx3^{GH/N}$ hypomorphs was 60% of that in $Tbx3^{+/+}$ (0.017 ± 0.001 mm^3 vs. 0.027 ± 0.003 mm^3; $P = 0.05$; Fig. S5), and in $Tbx3^{G/G}$ mutants it was 45% of that in $Tbx3^{+/+}$ (0.049 ± 0.017 mm^3 vs. 0.107 ± 0.024 mm^3; $P < 0.01$; Fig. S5). We investigated whether this was caused by decreased proliferation or increased cell death and found no significant difference between $Tbx3^{GH/N}$ and $Tbx3^{+/+}$ in the number of BrdU-positive cells in the Hcn4$^+$ SAN at E11.5 or E12.5, nor did we detect apoptosis. This agrees with previous studies (13, 21, 22) and suggests that a threshold of Tbx3 is required to establish and/or maintain cells with SAN identity. As the quantity of nodal tissue influences its ability to drive the surrounding myocardium (23, 24), we posit that bradycardia and atrial arrhythmias (Fig. 3 *C–E*) are related to the smaller SAN of *Tbx3* hypomorphic mutants.

To investigate molecular causes of lethal arrhythmias in $Tbx3^{GH/N}$ hypomorphs, we studied cardiac gene expression and compared it with that previously reported from $Tbx3^{Cre/Cre}$ mutants (13, 19). Expression patterns of known working myocardial genes *Cx40*, *Nppa*, *Tbx18*, and *Tnni3* mRNAs were not significantly changed in $Tbx3^{GH/N}$ E12.5 hearts. In contrast, *Cx43* is a direct target of Tbx3 repression (13) and was ectopically expressed at the crest of the ventricular septum in mutants (Fig. 2 *I–J*). This is the nascent AVB and a region where *Tbx3* mRNA and protein levels were severely decreased in $Tbx3^{GH/N}$ hypomorphic mutants (Fig. 2*H*). The expression patterns of *Hcn4*, *Tbx2*, *Tbx5*, and *Cacna2d2* (CCS markers) were preserved in $Tbx3^{GH/N}$ hypomorphs. These findings reveal that the level of residual *Tbx3* expression and protein function in
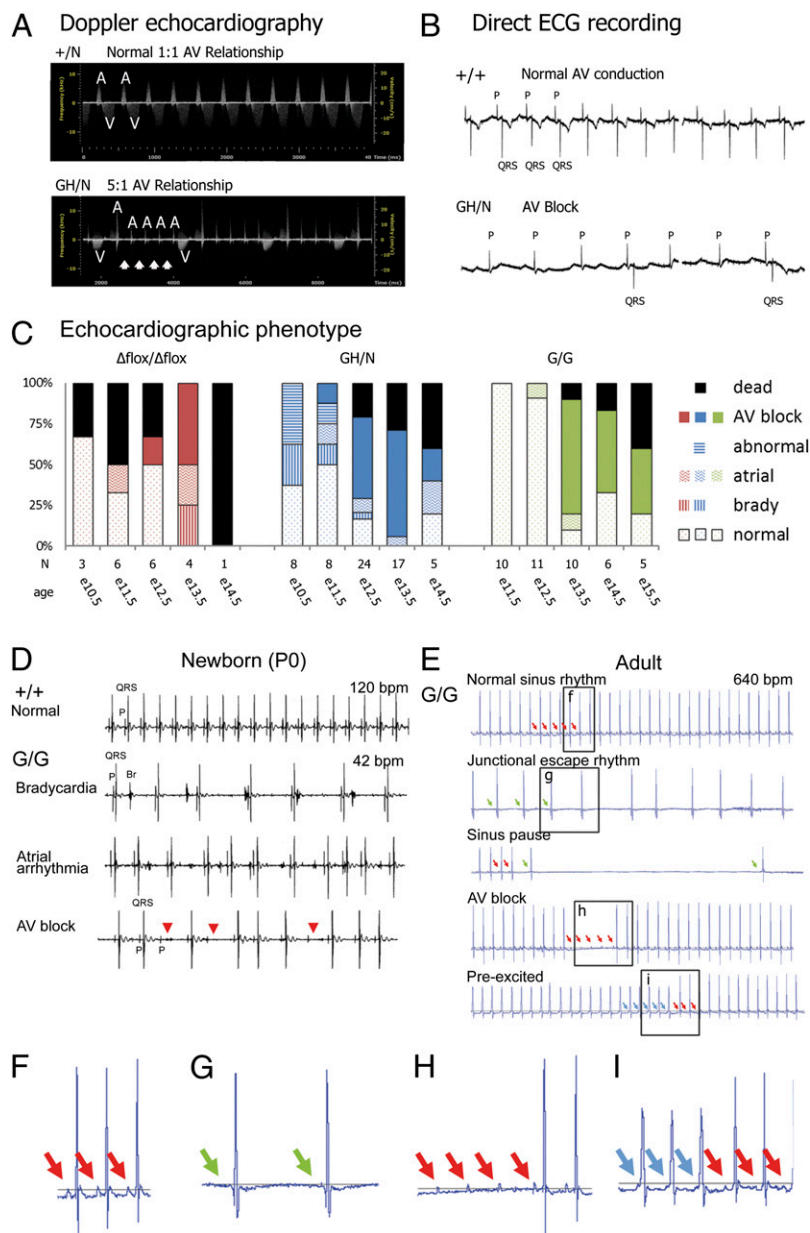
A Doppler echocardiography

+/N   Normal 1:1 AV Relationship

A A
V V

GH/N   5:1 AV Relationship

A A A A
V V

B Direct ECG recording

+/+   Normal AV conduction

P P P
QRS QRS QRS

GH/N   AV Block

P P P P P P P
QRS QRS

C Echocardiographic phenotype

Δflox/Δflox   GH/N   G/G

- dead
- AV block
- abnormal
- atrial
- brady
- normal

N: 3, 6, 6, 4, 1 | 8, 8, 24, 17, 5 | 10, 11, 10, 6, 5

age: e10.5, e11.5, e12.5, e13.5, e14.5 | e10.5, e11.5, e12.5, e13.5, e14.5 | e11.5, e12.5, e13.5, e14.5, e15.5

D Newborn (P0)

+/+   Normal   120 bpm
QRS
P

G/G   Bradycardia   42 bpm
QRS
P Br

Atrial arrhythmia

AV block
QRS
P P

E Adult

G/G   Normal sinus rhythm   640 bpm
f

Junctional escape rhythm
g

Sinus pause

AV block
h

Pre-excited
i

F **G** **H** **I**

Fig. 3. *Tbx3* mutants have multiple cardiac arrhythmias. (*A*) Doppler ultrasound recordings of blood flow velocity (*y* axis) vs. time (*x* axis) from E12.5 ventricles. Flow into the ventricle occurs during atrial contraction ("A"), and flow out of the ventricle during ventricular contraction ("V"). Normal 1:1 ratio of A and V is shown in *Tbx3*[+/N]. The *Tbx3*[GH/N] hypomorph has abnormal 5:1 and 4:1 ratios; the white arrows indicate A not followed by V. (*B*) Direct ECG recordings of E13.5 embryos: electrical activity (*y* axis) vs. time (*x* axis). *Tbx3*^{+/+} shows normal P wave (atrial depolarization) followed by QRS complex (ventricular depolarization); there is 1:1 AV conduction. In a *Tbx3*[GH/N] hypomorph, QRS occurs only after every third or fourth P wave (3:1 or 4:1 AV block). (*C*) Frequency of cardiac phenotypes detected by Doppler and 2D ultrasound. Abnormal, subtle change in cardiac appearance including bradycardia, dilated chambers or dyscoordinated contractions; AV block, A not followed by V; Atrial, irregular rhythm, but coordinated AV contractions; Brady, heart rate slower than 100 beats/min (bpm); Dead, embryos without a heartbeat; Normal, heart rate greater than 100 bpm and 1:1 AV conduction. (*D*) Multiple arrhythmias were detected in newborn *Tbx3*[G/G] mutants by direct ECG recordings. Br, breathing artifact; P, P wave; QRS, QRS complex. Red arrowhead indicates AV block, no QRS after a P wave. (*E*) Telemetric ECG recording revealed multiple types of arrhythmias in adult *Tbx3*[G/G] mutants. Red arrows indicate P waves (not all are marked). Green arrows indicate absence of a P wave (junctional escape beat). Blue arrows indicate a preexcited beat, detected by loss of the PR interval, fusion of the P and QRS complex, and a widened QRS (39). Boxed regions (*f*–*i*) are enlarged in *F*–*I*, and additional examples are in Fig. S4. Representative lead 1 tracings are shown.

Tbx3[GH/N] hypomorphs was sufficient to preserve most of the known complementary gene expression boundaries between working and conduction myocardium, but not to prevent CCS dysfunction and lethal arrhythmias.

In the rare surviving adult *Tbx3*[G/G] mutants, histology and connexin protein expression patterns of the CCS were so severely disrupted that no structures with the histologic or molecular identity of the SAN (Fig. 4 *G* and *J* vs. Fig. 4 *A* and *D*) or AVB (Fig. 4*L*

vs. Fig. 4 *C* and *F*) could be detected. These regions were abnormally positive for the working myocardial marker Cx43.

Dysregulation of Multiple Ion Channel Genes in *Tbx3*-Deficient AVC. The arrhythmias observed in *Tbx3*[GH/N] hypomorphs indicate that other genes besides those known to distinguish working and conducting myocardium are required for CCS function and must be disrupted by decreased levels of Tbx3. Given the overlapping

Table 1. Newborn cardiac function analysis

Function	$Tbx3^{+/+}$ ($n = 7$)	$Tbx3^{G/G}$ ($n = 9$)	P value
ECG, anesthetized			
HR, beats/min	151 ± 32	79 ± 29	0.001
QRS duration, ms	16 ± 1	21 ± 4	0.003
PR interval, ms	122 ± 19	111 ± 17	NS
Arrhythmias, N			
Bradycardia*	0	7	
Irregular atrial	0	5	
AV block	0	1	
Echo, awake			
N	19	12	
HR, beats/min	323 ± 61	259 ± 73	0.01
FS (%)	48 ± 6	54 ± 7	0.02
LVID, systole, mm	0.67 ± 0.11	0.62 ± 0.11	NS
LVID, diastole , mm	1.29 ± 0.13	1.36 ± 0.25	NS
LVW, systole, mm	0.43 ± 0.07	0.47 ± 0.08	NS
LVW, diastole, mm	0.34 ± 0.08	0.39 ± 0.10	NS

Echo, echocardiography; FS, fractional shortening; HR, heart rate; LVID, left ventricle inner diameter; LVW, left ventricular wall thickness; NS, not significant.
*HR < 100 beats/min.

expression of *Tbx2* and *Tbx3* in the AVC (19, 25), the linkage of *Tbx5* and *Tbx3*, and the known role of Tbx2 and Tbx5 in CCS function (1, 6, 26), we determined expression of *Tbx2* and *Tbx5* by quantitative RT-PCR (qRT-PCR) in E10.5 whole hearts, and in microdissected E12.5 atrial/AVC tissue in our allelic series of *Tbx3* mutants. We detected no changes in the levels of these transcripts (Figure S6 *A and B*).

We performed an unbiased, genome-wide expression analysis with Agilent microarrays to identify dysregulated genes downstream of Tbx3 that could be involved in the molecular bases of embryonic AV block. Gene profiles from AVC tissue before arrhythmia onset (E10.5) of $Tbx3^{GH/N}$ hypomorphs and $Tbx3^{+/+}$ controls was compared (array data deposited in Gene Expression Omnibus database; accession no. GSE24122). Analysis revealed 958 transcripts significantly changed by more than 1.5 fold.

We validated the microarray findings by using qRT-PCR to assay genes related to ion handling, with known cardiac expression, or relevant to AVC development or conduction (1, 3, 4). As expected, *Tbx3* was strongly decreased (−6.6-fold change by

qRT-PCR) in $Tbx3^{GH/N}$ hypomorphs. A number of genes with the potential to affect conduction system function were highly dysregulated in $Tbx3^{GH/N}$ mutant AVC. Transcripts for *Kcne3* (8.5-fold), a potassium channel regulatory subunit; *Chac1* (7.1-fold), a cation transport regulator-like protein; *Adora2a* (2.3-fold), encoding the adenosine 2A receptor, which contributes to heart rate regulation in adult mice (27); *Kcnj4* (1.9-fold), encoding a potassium channel; and *Atp1b4* (1.8 fold), encoding a sodium-potassium ATPase, were all significantly increased. *Scn7a* (−3.5-fold), a voltage-gated sodium channel; *Gjc1* (−1.5-fold), which encodes the slowly conducting gap junction Cx30.2; *Atp1a2* (−1.5-fold), encoding a sodium-potassium ATPase; and *Nkx2.5* (−2.8-fold) and *Gata4* (−1.6-fold), which have demonstrated roles in human and mouse arrhythmias (1, 6), were decreased. *Bmp10*, *Irx1*, *Irx3*, *Tnni2*, *Nppa*, *and Nppb* transcripts are expressed in trabeculated ventricular working myocardium (28–31); however, consistent with our hypothesis that Tbx3 is required for establishing the identity of CCS myocardium (as detailed earlier and in refs. 13, 19), transcript levels for these genes were increased in the $Tbx3^{GH/N}$ AVC. Periostin, encoded by *Postn*, is expressed by the AV valve progenitor cells in the AV cushions (32). Decreased *Postn* transcripts (−2-fold) in $Tbx3^{GH/N}$ AVC may directly result from decreased Tbx3 in AV cushion mesenchyme (included in the tissue assayed), or reflect altered signaling from AVC myocardium to valve progenitors.

We compared transcript levels of the four most dysregulated genes between the AVC and LV to examine differential regulation in these two tissues (Fig. S6C). The transcript levels of *Tbx3*, *Kcne3*, and *Scn7a* were lower, and *Chac1* levels were higher, in WT LV vs. AVC. These relationships were preserved in $Tbx3^{GH/N}$ hypomorphs, indicating that, whether *Kcne3*, *Chac1*, and *Scn7a* are direct or indirect targets of Tbx3 regulation, Tbx3 deficiency affects their expression similarly in both tissues.

Conditional Disruption of *Tbx3* at Multiple Locations in AV Conduction System Causes Embryonic AV Block. To determine which Tbx3⁺ regions are required for normal embryonic AV conduction, we used two spatially restricted Cre lines, *Mef2c*-AHF-Cre and *cGata6*-Cre (33, 34), and our unique *Tbx3* conditional floxed allele (*Tbx3^flox*; Fig. 1*A*) to generate *Tbx3* conditional mutant embryos. We visualized the entire Tbx3⁺ myocardial population (Fig. 5 *A–C*), using the conditional *Tbx3* GFP reporter allele (*Tbx3^G*) recombined with *αMHC*-Cre (35) and compared the GFP-positive domains to those detected with the mT/mG re-

Table 2. Adult ECG parameters and arrhythmias

Parameter	$Tbx3^{+/+}$ ($n = 7$)	$Tbx3^{G/+}$ ($n = 4$)	$Tbx3^{G/G}$ ($n = 17$)	P value	Definitions
Anesthetized mice					
HR, beats/min	365 ± 33	396 ± 24	360 ± 79	NS	—
QRS duration, ms	19 ± 2	16 ± 4	21 ± 6	NS	—
PR interval, ms	38 ± 4	38 ± 3	25 ± 9	0.001	—
Awake mice: telemetry					
No. of mice	5	—	10	—	—
HR, beats/min	691 ± 18	—	608 ± 106	0.06	—
QRS duration, ms	13 ± 0.7	—	15 ± 1.8	0.04	—
PR interval, ms	30 ± 1.3	—	25 ± 5.3	0.06	—
Arrhythmias, N					
Bradycardia	0	—	3	—	HR range <600
Sinus pauses	0	—	5	—	>10/h
PACs	0	—	2	—	>1/h
Preexcitation	0	—	5	—	—
Junctional rhythm	0	—	1	—	—
2 °AV block	0	—	2	—	>10/h
PVCs	0	—	5	—	>1/h

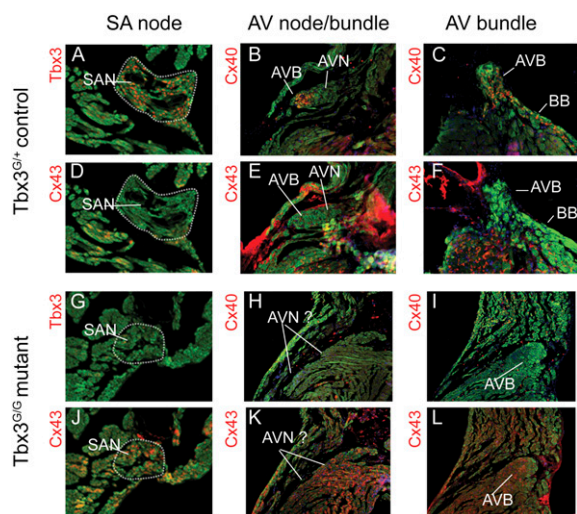HR, heart rate; PAC, premature atrial contraction; PVC, premature ventricular contraction.

Fig. 4. Histologic conduction system abnormalities in adult *Tbx3^G/G^* mutants. IHC for protein indicated at upper left corners of panels (red on green tissue background). Tbx3 is undetectable in the mutant SAN (*G* vs. *A*); Cx43 is ectopically expressed (*J*). In controls, Cx40 is expressed in the AVB and BB and excluded from the AVN (*B* and *C*), whereas Cx43 is excluded from the SAN (*D*), AVN, AVB, and BB (*E* and *F*). In the mutant, no AVN can be identified (*H* and *K*). The AVB and BB can be identified histologically in the mutant by its position at the crest of the ventricular septum and the surrounding connective tissue, but Cx40 protein is not detected (*I*) and Cx43 is ectopically expressed (*K* and *L*). BB, bundle branch.

porter (36) after Cre activity from *Mef2c*-AHF-Cre or *cGata6*-Cre. *Mef2c*-AHF-Cre is active in the right ventricle and outflow tract, including the ventricular septal crest (nascent AVB), but not in the AVC myocardium (nascent AV node; Fig. 5 *D–F*) (34, 37). A total of 75% (*n* = 9) of *Tbx3^flox/flox^*;*Mef2c*-AHF-Cre mutants echoed from E12.5 to E13.5 had AV block or were dead, whereas all littermates had normal AV conduction (Table 3). *cGata6*-Cre activity is restricted to and variable within AVC myocardium (33) (Fig. 5 *G–L*). AV block was detected in 67% (*n* = 6) of *Tbx3^flox/flox^*;*cGata6*-Cre embryos echoed from E12.5 to E14.5 but not in littermates (Table 3), implicating the AVC myocardium in arrhythmia pathogenesis. Normal rhythm in 33% of *Tbx3^flox/flox^*;*cGata6*-Cre embryos is likely attributable to variable Cre activity (33). Thus, AV block occurs after disruption of *Tbx3* from either of two distinct domains of the developing CCS: the nascent AVB or AVC myocardium, which contains the nascent AV node.

Conditional Knockdown of *Tbx3* in Adults Causes Second-Degree AV Block. *Tbx3* is expressed in adult CCS tissues (13), leading us to question whether Tbx3 has roles in maintaining structure or function of the mature CCS. To address this, we used an inducible, globally expressed Cre-recombinase (CAGGCre-ER) (38). We administered tamoxifen to *Tbx3^flox/flox^*;CAGGCre-ER (*n* = 5) and littermate controls (*n* = 3) at 2 to 3 mo of age and monitored their cardiac rhythms before, during, and weekly for 10 wk after tamoxifen induction by using telemetric ECG. Telemetry data were mined for changes in heart rate, ECG intervals, and arrhythmias.

Rhythm abnormalities observed in adult conditional mutants included an increased incidence of second-degree AV block (Fig. 6 *A* and *B*) and sinus pauses (Fig. S7). Second degree AV block was rarely seen in control mice (*Tbx3^+/+^*;CAGGCre-ER and *Tbx3^flox/flox^*); they had, at most, three episodes per hour of AV block, and no increase after tamoxifen treatment. This indicates that neither tamoxifen nor the Cre genotype causes AV block. Baseline incidence of AV block or sinus pauses (before tamox-

ifen) was not different in *Tbx3^flox/flox^*;CAGGCre-ER mutants compared with controls. After tamoxifen treatment, we observed an increased frequency of AV block within 1 wk, which peaked at 2 to 6 wk. The frequency of AV block decreased with time, and a statistically significant excess persisted in the mutants 9 and 10 wk after Cre induction (Fig. 6*B*). SAN pauses were more frequent in *Tbx3^flox/flox^*;CAGGCre-ER compared with controls (0–16 vs. 0–6 pauses per hour).

Two pairs of adult mutant (*Tbx3^flox/flox^*;CAGGCre-ER) and control (*Tbx3^flox/flox^*) animals were killed 2 wk after tamoxifen treatment to assess the impact on Tbx3 production by IHC. Although Tbx3 protein was not eliminated in the *Tbx3^flox/flox^*;CAGGCre-ER hearts, the number and density of Tbx3^+ cells was decreased in the region of the Hcn4^+ AV node and AVB (Fig. 6 *C–F*).

Discussion

Our studies electrically interrogate the developing CCS and delineate CCS dysfunction resulting from disruption of cell-autonomous *Tbx3* function. We discovered critical roles for Tbx3 in establishing and maintaining conduction tissue identity and function during development and adult life. Our data reveal that Tbx3 has unique and highly dosage-sensitive functions in the conduction system that cannot be compensated for by other factors, even Tbx2, which is highly related and coexpressed with Tbx3 in the AVC.

Our allelic series was integral to defining the dosage sensitive requirements for Tbx3 as exemplified by the multiple arrhythmia types observed in embryonic, newborn, and adult *Tbx3^G/G^* mutants compared with embryonic lethal AV block in *Tbx3^GH/N^* hypomorphs. The documented fetal defects in *Tbx3^G/G^* mutants include intermittent bradycardia and atrial arrhythmias, which are survivable, as 80% are recovered at birth. Intermittent AV block also occurs later in development than in the more hypomorphic *Tbx3^GH/N^* embryos, in which it is lethal. The very few *Tbx3^G/G^* mutants that survive to adulthood are clearly on the less severe side of the spectrum and nonetheless have marked histologic abnormalities (Fig. 4) and arrhythmias. In addition to sudden death in adult *Tbx3^G/G^* mutants, 50% of adult *Tbx3^G/G^* mutants exhibit what appears to be ventricular preexcitation, suggesting the existence of accessory AV conduction pathways. Normally, slow-conducting Tbx3^+ AVC myocardium is maintained around the valves and the annulus fibrosis is formed and further insulates the atrial and ventricular myocardium. Both are likely to be disrupted in the *Tbx3^G/G^* mutants, as was previously observed in mutants of the Bmp–Tbx2–Notch regulatory axis (39–41).

Further evidence of extreme dosage sensitivity of cardiac conduction to Tbx3 is that minor decrements in adult mice disrupt sinoatrial and AV conduction. Milder arrhythmias in *Tbx3^flox/flox^*;CAGGCre-ER compared with surviving adult *Tbx3^G/G^* mutants is likely caused by the presence of Tbx3 in some cells in *Tbx3^flox/flox^*;CAGGCre-ER mutants: both alleles of *Tbx3* were conditional, and Cre efficiency is variable with multiple loci (42, 43). Additionally, *Tbx3^G/G^* survivors have Tbx3 dysfunction throughout development. This is similar to Nkx2.5 mutants: juvenile gene ablation results in decreased severity and slower evolution of arrhythmias compared with both perinatal and embryonic ablation (44, 45). Interestingly, the peak and subsequent resolution of arrhythmia severity in the adult knocked-down animals suggests that conduction tissue can regenerate or reorganize to replace the function of *Tbx3*-depleted cells. Our data indicate that *Tbx3* is required for the homeostasis of the adult conduction tissues and may be a useful factor to harness in efforts for conduction tissue regeneration.

SA node hypoplasia coupled with frequent sinus pauses and junctional rhythms in *Tbx3^G/G^* mutants and atrial arrhythmias in *Tbx3^GH/N^* hypomorphs indicate that *Tbx3* is required during de-
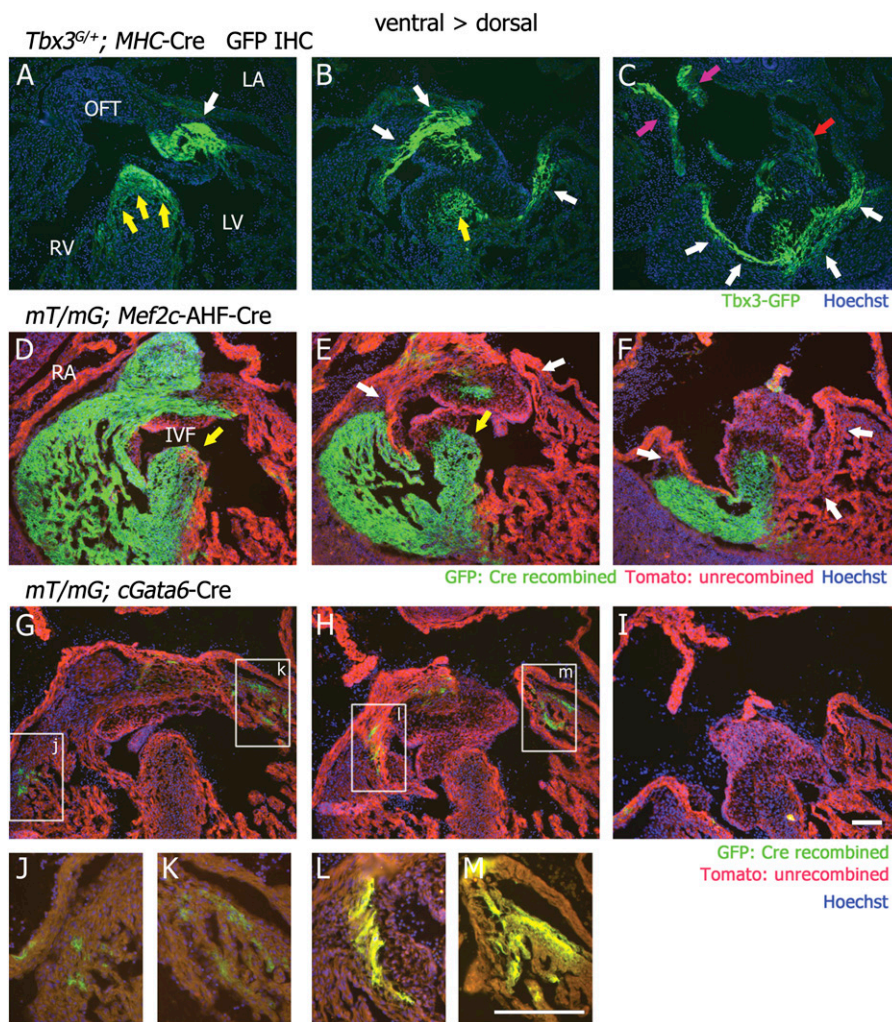
Fig. 5. A unique *Tbx3^flox* allele and tissue-restricted Cre recombination permit localization of Tbx3 expression domains responsible for embryonic AV block. (*A–C*) α-GFP IHC in E12.5 *Tbx3^{G/+}*;*αMHC-Cre* embryo reveals all myocardial Tbx3 expression domains: crest of the ventricular septum (yellow arrows), AVC myocardium (white arrows), base of atrial septum (red arrow), and venous valves (magenta arrows). (*D–M*) Direct fluorescence in *mT/mG* embryos after Cre-mediated recombination with *Mef2c-AHF-Cre* (*D–F*) or *cGata6-Cre* (*G–M*). *Mef2c*-AHF-Cre recombines in the OFT, right ventricle, and a portion of the crest of the ventricular septum (yellow arrows, nascent AVB); AVC myocardium is not recombined (white arrows). *cGata6*-Cre recombines a subset of AVC myocardial cells (from which the AVN forms). Higher magnification of the areas boxed in panels *G* and *H* are shown in *J–M*. Representative sections from ventral to dorsal through the heart for each series are shown. IVF, interventricular foramen; OFT, outflow tract. The legend to Fig. 2 includes other applicable abbreviations. (Scale bars: 100 μm.)

velopment for proper SAN size and function. Adequate SAN volume and electrical coupling to adjacent tissues are needed to drive surrounding myocardium (23, 24). SAN hypoplasia in human newborns has been linked to arrhythmias similar to those in *Tbx3^{G/G}* mutants (46, 47).

Our finding of AV block resulting in extreme ventricular bradycardia in utero explains the embryonic demise of *Tbx3^{GH/N}* hypomorphs. Mechanical activity detected by echocardiography was used as a surrogate measurement of electrical activity in the embryonic mice. Electrical conduction is usually translated into mechanical contraction, although in critically ill hearts, there are instances in which this translation is disrupted (called pulseless electrical activity). The direct measurements of electrical activity we performed by ECG on embryos confirmed that the rhythm disturbance detected by echocardiography was AV block rather than pulseless electrical activity of the intermittently noncontracting ventricle. Although we have made a major step forward in being able to use ECG in living embryos, the direct ECG measurement in embryos is highly invasive, embryo rhythm can be assessed only

briefly a single time, and only a few embryos from each litter can be evaluated before the mother becomes unstable. Thus, this technique alone is not sufficient to interrogate ongoing conduction system dysfunction over developmental time. Although echocardiography has traditionally been used for structural and hemodynamic parameters, we have found that rhythm abnormalities can be reliably detected and that AV block can be distinguished from other arrhythmias in embryonic mice. The intermittent nature of the AV block is consistent with the variable length of survival. Optical mapping of E12.5 *Tbx3^{Cre/Cre}* hearts demonstrated a normal AV conduction time (19). This phenotypic discrepancy may reflect differing dosages of Tbx3 protein or result from experimental differences: we detected AV block intermittently in vivo whereas optical mapping was performed on explanted hearts which is obviously a less physiologic setting and could easily miss intermittent dysfunction. Maternal anesthesia we used could unmask altered AV conduction in a genetically vulnerable substrate. Reproducible detection of AV block in *Tbx3* deficient and tissue-specific conditional mutants but never in littermates establishes the

Table 3. Arrhythmia phenotypes of *Tbx3* conditional mutants

Mutant	Phenotype	Mutants	Littermates
*Tbx3*flox/flox; c*Gata6*-Cre			
	Normal rhythm	2	40
	Atrial arrhythmias	0	4
	AV block	4	0
	Dead	0	0
*Tbx3*flox/flox; *Mef2c*-AHF-Cre			
	Normal rhythm	1	28
	Atrial arrhythmias	1	3
	AV block	3	0
	Dead	4	0

arrhythmogenicity of *Tbx3* deficiency, and genetically maps tissues responsible for AV block.

c*Gata6*-Cre recombines in the developing AVC myocardial precursors of the AVN and AV rings, whereas *Mef2c*-AHF-Cre is active in a broad domain including the developing ventricular septal crest (AVB precursors), but strictly excluding the AV ring and AV node (37). AV block occurs in both conditional mutants, and thus the lack of overlap in their Cre activity reveals that Tbx3 is required in multiple regions along the embryonic AV conduction axis.

Ion channels and connexons that determine the action potential shape and propagation velocity are composed of multiple subunits and regulatory proteins. Individual genes/proteins are expressed at very low levels, which makes the detection of alterations in heterogeneous tissues difficult. The complexity of ion channel and connexin expression within the conduction system itself, and the changes that occur throughout development, are not well understood at this time; it is highly unlikely that any one dysregulated factor will explain the complex phenotypes we observe. Our genome-wide expression analysis was designed to detect targets with the earliest and least redundant requirements for Tbx3. Dysregulation of genes with the potential for altering cardiac conduction, and of ventricular myocardial genes in the AVC of the *Tbx3* hypomorphs, suggests that the mutant myocardium fails to establish a normal conduction system molecular identity and is consistent with the observed arrhythmias. There were markedly increased levels of *Kcne3* and *Chac1*, and decreased levels of *Scn7a* transcripts. *Kcne3* encodes the MiRP2 potassium channel regulatory subunit, which markedly alters the function of at least three voltage-gated potassium channels important in cardiac conduction (48). Ectopic expression of Kcne3 accelerates repolarization and increases heart rate (49). *Chac1* encodes a minimally characterized cation transport regulator-like protein. *Scn7a* encodes a voltage-gated sodium channel with a role in nervous system-controlled sodium and water homeostasis (50). The demonstrated and theoretical functions of the encoded proteins suggest that *Kcne3*, *Chac1*, and *Scn7a* are Tbx3 targets whose misexpression disrupts conduction in the developing embryonic heart. Function of these genes in conduction versus working myocardium and effects on ion trafficking merit future investigation.

Exquisite sensitivity of the developing and mature CCS to *Tbx3* dosage is similar to that demonstrated previously for *Tbx1* and *Tbx5* with regard to cardiac morphogenesis (26, 51). Notably, there is little genotype–phenotype correlation as to type/ severity of defects in human *TBX* mutation syndromes. Phenotypic variations in familial pedigrees may reflect this dosage sensitivity, the effects of modifier loci, as well as complex interactions between T-box proteins and other transcription factors thus far only superficially delineated.

Arrhythmias and their resolution in adult *Tbx3* conditional mutants make Tbx3 a potential factor for efforts to regenerate
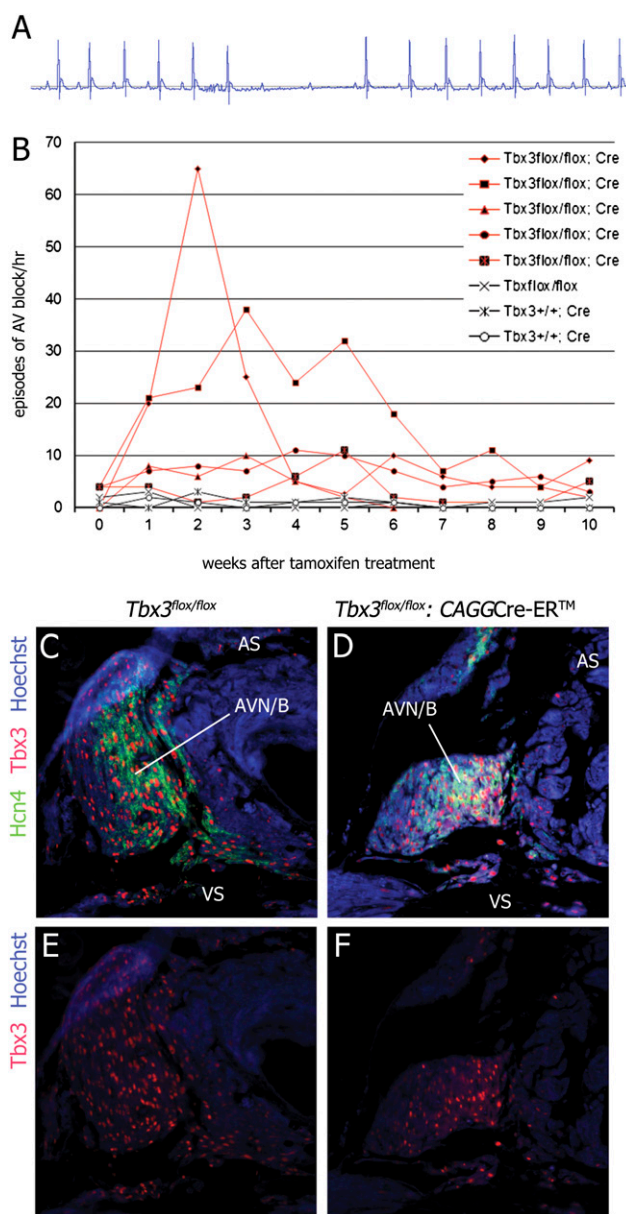
Frank et al.

Fig. 6. Adult *Tbx3* knockdown causes AV block. (*A*) AV block detected by telemetric ECG of *Tbx3*flox/flox;*CAGG*Cre-ERTM adult mice after tamoxifen treatment. (*B*) AV block frequency in individual mice (*y* axis) from 2 h of weekly data after tamoxifen treatment (*x* axis). Red lines connect data from knockdown animals. Black lines from control animals of indicated genotypes. (*C–F*) αTbx3 and αHcn4 IHC in AV node and AVB area of control and Tbx3 knockdown adult. Hcn4⁺ staining localizes the AV conduction tissue (*C* and *D*). Tbx3 protein in *Tbx3*flox/flox control (*E*). Tbx3 protein persists in some cells in the *Tbx3*flox/flox;*CAGG*Cre-ERTM mouse after tamoxifen treatment (*F*). Similar locations within the AV node/AVB area are shown.

conduction tissue. Our findings indicate that *TBX3* and its targets merit investigation as candidate genes for human arrhythmia syndromes.

Materials and Methods

Mice. Three targeted mutations of *Tbx3* were generated in mice: a null allele (*Tbx3*^{N}), a hypomorphic allele (*Tbx3*^{GH}), and a floxed conditional allele (*Tbx3*^{flox}). Additional alleles were generated by recombining the GH and flox alleles with FLPe or Cre-recombinase (*Tbx3*^{G} and *Tbx3*$^{\Delta flox}$, respectively). Lines were maintained on a 50% C57BL/6, 50% SV129 background for embryo and newborn studies, and crossed into FVB (25% C57BL/6; 25% SV129;

50% FVB) for adult studies. Experiments were conducted in compliance with institutional animal care and use committee standards.

Generation of Targeted *Tbx3* Alleles. *Tbx3^N* has a 4.6-kb deletion starting from an EcoRI site 920 bp 5′ of the translational start site (ATG) to an EcoRI site 3.7 kb 3′ of the ATG, deleting exons 1 to 3. The targeting vector also included a FRT-flanked neomycin (neo^r) selection cassette at the BglII site 3.2 kb 5′ of the ATG.

The *Tbx3^GH* allele contains a loxA2 site inserted into the BamHI site 5.4 kb 3′ of the ATG. An FRT-flanked hygromycin resistance gene, a second loxA2 sequence, and a splice acceptor/GFP were inserted in an Apa1 site approximately 14 kb 3′ of the ATG. The hygromycin gene was removed by using the FLPe transgene (52) generating *Tbx3^G*. These alleles express a Tbx3-GFP fusion protein after Cre-mediated recombination.

Tbx3^flox contains two loxP sequences inserted in parallel orientation flanking the first exon of the *Tbx3* gene. Cre-mediated recombination generates the *Tbx3^Δflox* null allele. *Tbx3^flox/flox* mice survive, have normal limbs, and reproduce normally.

Cre Mouse Lines. Transgenic Cre lines used for conditional ablation of *Tbx3* included: deleter-Cre (16), Mef2c-AHF-Cre (34), cGata6-Cre (33), αMHC-Cre (35), and CAGGCre-ER (38). Activities of these Cre lines in our mice were determined by using mT/mG and *Rosa26^lacZ* reporter mice (36, 53). CAGGCre-ER was induced by oral gavage of 0.25 mg/g tamoxifen (Sigma Chemical) in peanut oil (10 mg/mL) daily for four doses.

Genotyping. Genotypes were determined by PCR of genomic DNA from ear biopsies or yolk sacs; primer sequences are available upon request. "E" refers to days of gestation beginning from midnight on the day of identification of a copulation plug.

Echocardiography. Embryos were imaged in utero by using ultrasound biomicroscopy (Vevo 660; VisualSonics) with a 40-MHz transducer and 23-MHz spectral pulsed-wave Doppler. Heart rate and rhythm were determined from pulsed Doppler waveforms. Ventricular function was determined by fractional area change between systole and diastole from 2D images. Maternal anesthesia was achieved with 1% to 2% isoflurane, maintaining heart rate between 450 and 550 beats/min and rapid shallow breathing. Body temperature was maintained within normal range and duration of maternal anesthesia was less than 1.5 h. Hemodynamics of E10.5 to E15.5 embryos were analyzed at daily intervals. During scanning, the bladder was used as a reference point for the left and right uterine horns, and the relative location of embryos was mapped. After the final scan, laparotomy was performed, and position of the embryos correlated with ultrasound embryo location before genotyping. Newborn mice were studied awake on the morning of their birth. A short-axis view of the ventricles was obtained to determine wall and chamber dimensions.

Electrocardiogram Analysis. A unique method to record embryonic ECGs used 240-mm-diameter silver electrodes positioned around the thorax of embryos exposed through abdominal and uterine incisions leaving placental circulation intact; a ground electrode was attached to the anesthetized mother. For newborns and adults, needle electrodes were inserted into proximal limb skin under anesthesia. Electrodes were connected to a DC-powered differential amplifier; signals were filtered at 50 kHz and digitized at 10 kHz with a 12-bit A/D converter (Digidata 1322A; Molecular Devices). Data acquisition/analyses were performed with pClamp software (Molecular Devices).

Long-term ECG monitoring in adults was via two lead telemetry devices (Data Sciences International) implanted intraperitoneally. In hypomorphs and controls, we ascertained 24 h of data 4 d after implantation. For adult *Tbx3* conditional ablations and controls, we implanted telemetry devices at 2 mo of age; baseline data were obtained 4 d after implantation, and tamoxifen administration began 1 wk after implantation. Heart rhythm was monitored for 2 h each week for 10 wk after tamoxifen dosing. ECG data were analyzed using Ponemah Physiology Platform software (Data Sciences International).

In Situ Hybridization and Immunohistochemistry. Tissues were fixed in 4% paraformaldehyde, embedded in paraplast or frozen in optimal cutting temperature compound, and sectioned at 7 to 10 μm for immunohistochemistry (IHC) and at 10 to 14 μm for in situ hybridization. Probes and methodology of in situ hybridization were described previously (12, 22, 25, 54). Immunohistochemistry was performed with Antigen Unmasking Solution (Vector Labs). Blocking solution consisted of 5% serum (specific to species of secondary anti-

body) and 0.3% Triton X-100 in PBS solution. Detection was with fluorescent-tagged or biotinylated secondary antibodies [detected with Vectastain Elite ABC reagent (Vector Labs) and ImmPACT DAB (Vector Labs) with eosin or methyl green counterstains]. For fluorescent IHC, nuclei were stained using Hoechst 33342 (H1399, 1:500 in PBS solution; Molecular Probes). Antibody combinations used included: anti-PECAM1 (553370; BD Biosciences) with biotin goat anti-rat Ig (559286, 1:75; BD Pharmingen), anti-BrdU (ab6326, 1:1,000; Abcam) with biotin-SP–conjugated donkey anti-rat IgG (712–065-153, 1:250; Jackson ImmunoResearch), or Alexa Fluor 594 goat anti-rat IgG (A11007, 1:500; Invitrogen), anti-Cx43 (C6219, 1:500; Sigma) with Alexa Fluor 488 goat anti-rabbit IgG (A11008, 1:500; Invitrogen), anti-Cx43 (45256, 1:200; BD Biosciences) with Alexa Fluor 568 donkey anti-mouse IgG (1:250), anti-GFP (A11122, 1:1,000; Invitrogen) with Alexa Fluor 488 goat anti-rabbit IgG (1:500), anti-Hcn4 (APC-052, 1:500; Alomone) with biotin goat anti-rabbit Ig (550338; BD Pharmingen), anti-Hcn4 (NG164345, 1:200; Millipore) with Alexa Fluor 488 donkey anti-rabbit IgG (1:250), anti-Tbx3 (SC17871, 1:500; Santa Cruz) with biotinylated rabbit anti-goat IgG (BA-5000, 1:500; Vector Labs), anti-Tbx3 (B1006, 1:200; Santa Cruz) with biotinylated donkey anti-goat (1:250) detected with TSA Enhancement Kit (NEL702A; Perkin-Elmer), and anti-Cx40 (K2204, 1:200; Santa Cruz) with Alexa Fluor 680 donkey anti-goat IgG (1:250). Apoptosis was assayed in paraffin-embedded sections by using the ApopTag Detection Kit (Chemicon). Embryos bearing the double fluorescent mT/mG Cre reporter were cryosectioned and directly imaged under epifluorescence (36).

Preparation of RNA and cDNA for Microarray and qRT-PCR. We assayed mRNA levels of *Tbx3*, *Tbx2*, and *Tbx5* in dissected atria and AVC tissues from E12.5 embryos with normalization to *hprt* by qRT-PCR.

For the microarray expression analysis, we microdissected AVC, including AV cushions and myocardium, from E10.5 *Tbx3^GH/N* mutant and *Tbx3^+/+* control embryos. Tissues were dissected in ice-cold PBS solution and stored in RLT buffer (Qiagen) at −80 °C. Five specimens of each genotype were pooled per sample. Total RNA was extracted from samples (RNeasy Micro Kit; Qiagen). The experiment was run in quadruplicate (four separate biologic replicates) on Agilent mouse whole-genome expression arrays. Agilent two-color LRILAK labeling, the Agilent two-color GE hybridization/wash protocol, and the Agilent 5-μm XDR scanning protocols were carried out the by the University of Utah Microarray Core Facility. The array image data were quantified using Agilent Feature Extraction software (version 9.5.1.1). Subtle intensity-dependent bias was corrected with LOWESS normalization, with no background subtraction. The raw and normalized data sets have been submitted to Gene Expression Omnibus database (accession no. GSE24122). Spots with intensity below background were removed before statistical analysis. Statistical analysis of normalized log-transformed data was performed in GeneSifter (www.geospiza.com).

For qRT-PCR validation, separate samples were made from tissue specimens obtained as described earlier. One hundred micrograms of total RNA was transcribed to cDNA by using the SuperScript III First-Strand Synthesis System (Invitrogen). Quantitative PCR was performed with iQ SYBR Green Supermix on the iCycler system (Bio-Rad), and normalization was to *hprt*, *gapdh*, and *β-actin*. Primer sequences provided upon request.

Statistics. Quantitative PCR data are presented using the ΔΔC(t) method (55). For the experiments evaluating expression of levels of *Tbx3* in the allelic series, ANOVA was performed with Student–Newman–Keuls testing to determine differences between individual groups. *t* tests were used to compare qRT-PCR measurements for Tbx3^GH/N vs. Tbx3^+/+ validation of microarray results. ECG and echocardiogram measurements were compared by using the Mann–Whitney *U* test or *t* test. Statistical analysis was performed by using SPSS Statistics (version 17.0); a significance level of 0.05 was used.

www.manaraa.com

1. Christoffels VM, Smits GJ, Kispert A, Moorman AF (2010) Development of the pacemaker tissues of the heart. *Circ Res* 106:240–254.
2. Horsthuis T, et al. (2009) Gene expression profiling of the forming atrioventricular node using a novel tbx3-based node-specific transgenic reporter. *Circ Res* 105:61–69.
3. Marionneau C, et al. (2005) Specific pattern of ionic channel gene expression associated with pacemaker activity in the mouse heart. *J Physiol* 562:223–234.
4. Schram G, Pourrier M, Melnyk P, Nattel S (2002) Differential distribution of cardiac ion channel expression as a basis for regional specialization in electrical function. *Circ Res* 90:939–950.
5. Hahurij ND, et al. (2008) Accessory atrioventricular myocardial connections in the developing human heart: Relevance for perinatal supraventricular tachycardias. *Circulation* 117:2850–2858.
6. Wolf CM, Berul CI (2006) Inherited conduction system abnormalities—one group of diseases, many genes. *J Cardiovasc Electrophysiol* 17:446–455.
7. Linden H, Williams R, King J, Blair E, Kini U (2009) Ulnar mammary syndrome and TBX3: Expanding the phenotype. *Am J Med Genet A* 149A:2809–2812.
8. Bamshad M, et al. (1997) Mutations in human TBX3 alter limb, apocrine and genital development in ulnar-mammary syndrome. *Nat Genet* 16:311–315.
9. Meneghini V, Odent S, Platonova N, Egeo A, Merlo GR (2006) Novel TBX3 mutation data in families with ulnar-mammary syndrome indicate a genotype-phenotype relationship: Mutations that do not disrupt the T-domain are associated with less severe limb defects. *Eur J Med Genet* 49:151–158.
10. Hasdemir C, et al. (2010) Transcriptional profiling of septal wall of the right ventricular outflow tract in patients with idiopathic ventricular arrhythmias. *Pacing Clin Electrophysiol* 33:159–167.
11. Pfeufer A, et al. (2010) Genome-wide association study of PR interval. *Nat Genet* 42:153–159.
12. Hoogaars WM, et al. (2004) The transcriptional repressor Tbx3 delineates the developing central conduction system of the heart. *Cardiovasc Res* 62:489–499.
13. Hoogaars WM, et al. (2007) Tbx3 controls the sinoatrial node gene program and imposes pacemaker function on the atria. *Genes Dev* 21:1098–1112.
14. Davenport TG, Jerome-Majewska LA, Papaioannou VE (2003) Mammary gland, limb and yolk sac defects in mice lacking Tbx3, the gene mutated in human ulnar mammary syndrome. *Development* 130:2263–2273.
15. Ribeiro I, et al. (2007) Tbx2 and Tbx3 regulate the dynamics of cell proliferation during heart remodeling. *PLoS ONE* 2:e398.
16. Schwenk F, Baron U, Rajewsky K (1995) A cre-transgenic mouse strain for the ubiquitous deletion of loxP-flanked gene segments including deletion in germ cells. *Nucleic Acids Res* 23:5080–5081.
17. Lüdtke TH, Christoffels VM, Petry M, Kispert A (2009) Tbx3 promotes liver bud expansion during mouse development by suppression of cholangiocyte differentiation. *Hepatology* 49:969–978.
18. Moon A (2008) Mouse models of congenital cardiovascular disease. *Curr Top Dev Biol* 84:171–248.
19. Bakker ML, et al. (2008) Transcription factor Tbx3 is required for the specification of the atrioventricular conduction system. *Circ Res* 102:1340–1349.
20. Mesbah K, Harrelson Z, Théveniau-Ruissy M, Papaioannou VE, Kelly RG (2008) Tbx3 is required for outflow tract development. *Circ Res* 103:743–750.
21. Mommersteeg MT, et al. (2007) Molecular pathway for the localized formation of the sinoatrial node. *Circ Res* 100:354–362.
22. Wiese C, et al. (2009) Formation of the sinus node head and differentiation of sinus node myocardium are independently regulated by Tbx18 and Tbx3. *Circ Res* 104:388–397.
23. Dobrzynski H, Boyett MR, Anderson RH (2007) New insights into pacemaker activity: promoting understanding of sick sinus syndrome. *Circulation* 115:1921–1932.
24. Joyner RW, van Capelle FJ (1986) Propagation through electrically coupled cells. How a small SA node drives a large atrium. *Biophys J* 50:1157–1164.
25. Aanhaanen WT, et al. (2009) The Tbx2+ primary myocardium of the atrioventricular canal forms the atrioventricular node and the base of the left ventricle. *Circ Res* 104:1267–1274.
26. Mori AD, et al. (2006) Tbx5-dependent rheostatic control of cardiac gene expression and morphogenesis. *Dev Biol* 297:566–586.
27. Yang JN, Chen JF, Fredholm BB (2009) Physiological roles of A1 and A2A adenosine receptors in regulating heart rate, body temperature, and locomotion as revealed using knockout mice and caffeine. *Am J Physiol Heart Circ Physiol* 296:H1141–H1149.
28. Chen H, et al. (2004) BMP10 is essential for maintaining cardiac growth during murine cardiogenesis. *Development* 131:2219–2231.
29. Christoffels VM, Keijser AG, Houweling AC, Clout DE, Moorman AF (2000) Patterning the embryonic heart: Identification of five mouse Iroquois homeobox genes in the developing heart. *Dev Biol* 224:263–274.
30. Tamura N, et al. (2000) Cardiac fibrosis in mice lacking brain natriuretic peptide. *Proc Natl Acad Sci USA* 97:4239–4244.
31. Zhu L, et al. (1995) Developmental regulation of troponin I isoform genes in striated muscles of transgenic mice. *Dev Biol* 169:487–503.
32. Norris RA, et al. (2009) Periostin promotes a fibroblastic lineage pathway in atrioventricular valve progenitor cells. *Dev Dyn* 238:1052–1063.
33. Davis DL, et al. (2001) A GATA-6 gene heart-region-specific enhancer provides a novel means to mark and probe a discrete component of the mouse cardiac conduction system. *Mech Dev* 108:105–119.
34. Verzi MP, McCulley DJ, De Val S, Dodou E, Black BL (2005) The right ventricle, outflow tract, and ventricular septum comprise a restricted expression domain within the secondary/anterior heart field. *Dev Biol* 287:134–145.
35. Abel ED, et al. (1999) Cardiac hypertrophy with preserved contractile function after selective deletion of GLUT4 from the heart. *J Clin Invest* 104:1703–1714.
36. Muzumdar MD, Tasic B, Miyamichi K, Li L, Luo L (2007) A global double-fluorescent Cre reporter mouse. *Genesis* 45:593–605.
37. Aanhaanen WT, et al. (2010) Developmental origin, growth, and three-dimensional architecture of the atrioventricular conduction axis of the mouse heart. *Circ Res* 107:728–736.
38. Hayashi S, McMahon AP (2002) Efficient recombination in diverse tissues by a tamoxifen-inducible form of Cre: A tool for temporally regulated gene activation/inactivation in the mouse. *Dev Biol* 244:305–318.
39. Aanhaanen WT, et al. (2011) Defective Tbx2-dependent patterning of the atrioventricular canal myocardium causes accessory pathway formation in mice. *J Clin Invest* 121:534–544.
40. Gaussin V, et al. (2005) Alk3/Bmpr1a receptor is required for development of the atrioventricular canal into valves and annulus fibrosus. *Circ Res* 97:219–226.
41. Rentschler S, et al. (2011) Notch signaling regulates murine atrioventricular conduction and the formation of accessory pathways. *J Clin Invest* 121:525–533.
42. Ma Q, Zhou B, Pu WT (2008) Reassessment of Isl1 and Nkx2-5 cardiac fate maps using a Gata4-based reporter of Cre activity. *Dev Biol* 323:98–104.
43. Watanabe Y, et al. (2010) Role of mesodermal FGF8 and FGF10 overlaps in the development of the arterial pole of the heart and pharyngeal arch arteries. *Circ Res* 106:495–503.
44. Briggs LE, et al. (2008) Perinatal loss of Nkx2-5 results in rapid conduction and contraction defects. *Circ Res* 103:580–590.
45. Takeda M, et al. (2009) Slow progressive conduction and contraction defects in loss of Nkx2-5 mice after cardiomyocyte terminal differentiation. *Lab Invest* 89:983–993.
46. Fox KM, Anderson RH, Hallidie-Smith KA (1980) Hypoplastic and fibrotic sinus node associated with intractable tachycardia in a neonate. *Circulation* 61:1048–1052.
47. Ho SY, Mortimer G, Anderson RH, Pomerance A, Keeling JW (1985) Conduction system defects in three perinatal patients with arrhythmia. *Br Heart J* 53:158–163.
48. Schroeder BC, et al. (2000) A constitutively open potassium channel formed by KCNQ1 and KCNE3. *Nature* 403:196–199.
49. Mazhari R, Nuss HB, Armoundas AA, Winslow RL, Marbán E (2002) Ectopic expression of KCNE3 accelerates cardiac repolarization and abbreviates the QT interval. *J Clin Invest* 109:1083–1090.
50. Watanabe E, Hiyama TY, Kodama R, Noda M (2002) NaX sodium channel is expressed in non-myelinating Schwann cells and alveolar type II cells in mice. *Neurosci Lett* 330:109–113.
51. Zhang Z, Baldini A (2008) In vivo response to high-resolution variation of Tbx1 mRNA dosage. *Hum Mol Genet* 17:150–157.
52. Rodríguez CI, et al. (2000) High-efficiency deleter mice show that FLPe is an alternative to Cre-loxP. *Nat Genet* 25:139–140.
53. Soriano P (1999) Generalized lacZ expression with the ROSA26 Cre reporter strain. *Nat Genet* 21:70–71.
54. Moorman AF, Houweling AC, de Boer PA, Christoffels VM (2001) Sensitive nonradioactive detection of mRNA in tissue sections: Novel application of the whole-mount in situ hybridization protocol. *J Histochem Cytochem* 49:1–8.
55. Livak KJ, Schmittgen TD (2001) Analysis of relative gene expression data using real-time quantitative PCR and the 2(-delta delta C(T)) method. *Methods* 25:402–408.

Frank et al.

www.manaraa.com